New Start-up Method for a Closed-Cycle Compression System with Gas Bearings and Its Characteristics

Huaqi Lian, Hong Wu, Yulong Li[*] and Chengjun Rong

Abstract

Gas bearings, which have the advantages of low frictional resistance and power loss, high rotational speed and high temperature operation, and long life, are more suitable than are traditional liquid lubricated bearings because of their high precision, high rotational speed, and special condition support. However, the problem of starting a closed-cycle compression system with gas bearings still needs to be solved for practical application. Thus, a new start-up method for a closed-cycle compression system with aerostatic gas bearings is proposed in this paper. Further, this paper presents a numerical simulation and experimental investigation of the method's feasibility and characteristics during the start-up process when the gas tank's initial pressure is fixed. The results show that the gas tank volume is approximately directly proportional to the start-up time allowable, and a gas tank volume sufficiently small, which not only ensures the feasibility of start-up, but also affects other components only slightly, can be obtained. A perfect combination of radial and axial loads also can be achieved to make the start-up time allowable as long as possible. R134a is a better choice for the working medium than is air, as the start-up time allowable is longer, which leads to a smaller gas tank. This research proposes a new start-up method for a closed-cycle compression system with aerostatic gas bearings which has sufficient load capacity to support system during the start-up method.

Keywords: Gas bearing, Start-up method, Gas tank, Start-up time allowable

1 Introduction

A gas bearing is one type of non-contact bearing that employs a pressurized gas film to support moving parts and resist external loads [1]. Compared to a liquid lubricated bearing, it has the advantages of low friction, limited heat generation and long life, which is due to the absence of contact between moving and stationary parts [2]. Moreover, no additional lubricant or coolant is required in the system with aerostatic bearings, since the air or the working medium are used for lubrication [3]. Therefore, theoretical research on gas bearings and their application has developed rapidly [4]. In theoretical research, Belforte approximated discharge coefficients of different restrictor for aerostatic thrust bearings by an experimental formula [5]. Then, based on the Belforte's research, Song et al. [6] used a FEM model to analyze the discharge coefficients considering the rotational speed, and Zhang et al. [7] study the discharge coefficients with consideration of the airflow status. Wang found temperature zone in which the stability of micro gas thrust bearing system is the weakest by analysis of dynamic characteristics of the system at high operating temperature up to 1600 K [8]. Zhang investigated the undesirable pressure depression in aerostatic thrust bearing and explored the condition on which the pressure depression occurs [9]. Obviously, the theoretical research becomes detailed. It's because gas bearing is widely used in various systems, such as spacecraft [10], satellite tests [11], turbomachine [12], medical equipment [13], computer memory devices [14], and precision machine tools [15],

*Correspondence: liyulong1897@sina.com
National Key Laboratory of Science and Technology on Aero Engines
Aero-thermodynamics & Collaborative Innovation Center for Advanced
Aero-Engine, School of Energy and Power Engineering, Beihang
University, Beijing 100191, China

by different institutions and companies. NASA has applied gas bearing widely in the aerospace field [16], for example, Dellacorte studied design and performance of gas foil bearing [17] and applied them to the turbine engine [18], while Demag in Germany and Nakanishi in Japan have applied gas bearings to spindles and introduced typical products.

In gas bearings' application, the working medium and the system based on the bearings become diverse [19]. In recent years, a closed-cycle compression system with gas bearing has become popular [20]. Marsh et al. [21] conducted experiments to compare the influence of lubrication mixed with different ingredients (helium, neon, argon, etc.) on gas bearings' stiffness and the rotors' vibration. Briggs et al. [22] compared power loss with helium, nitrogen, and carbon dioxide from atmospheric pressure to 4.83 MPa and at shaft speeds from 10 kr/min to 42 kr/min. Conboy et al. [23] created a model that considered the real gas effect to predict the pressure field in a thrust bearing lubricated by high pressure carbon dioxide in a closed-cycle, supercritical carbon dioxide turbine. Schiffmann designed a thermally driven heat pump with gas bearing based on the combination of a heat pump cycle and an organic Rankine cycle [24], and investigated the effect of the occurrence of condensation in the gas film near saturation conditions [25]. Obviously, it is a research hotspot that applying gas bearings with working mediums other than air in the closed-cycle compression system, but few papers focus on the gas bearing with Freon, which is one of points in this paper.

The closed-cycle compression system with gas bearings reduces complexity. However, another potential problem arises—that the gas bearing is unable to withstand the load without an extended air compressor—which is referred to as a start-up problem [26]. Using an aerodynamic gas bearing to support the rotor is one solution to this problem [27]. However, there is still friction between the gas bearings and rotors during the start-up process [28], which makes the problem severe if the system needs to be started and stopped frequently.

Therefore, to solve this problem, this paper proposes a new method to start-up a closed-cycle compression system with aerostatic gas bearings. Then, a mathematical model is established to simulate the characteristics found during the start-up process, and a test bench is built to verify the simulation.

2 Start-up Method
An ordinary system with gas bearings is shown in Figure 1(a). The system consists of a shaft, compressor, several journal gas bearings (JGB) and thrust gas bearings (TGB), an external air compressor, an air filter, and valves. The gas bearings' supply and exhaust
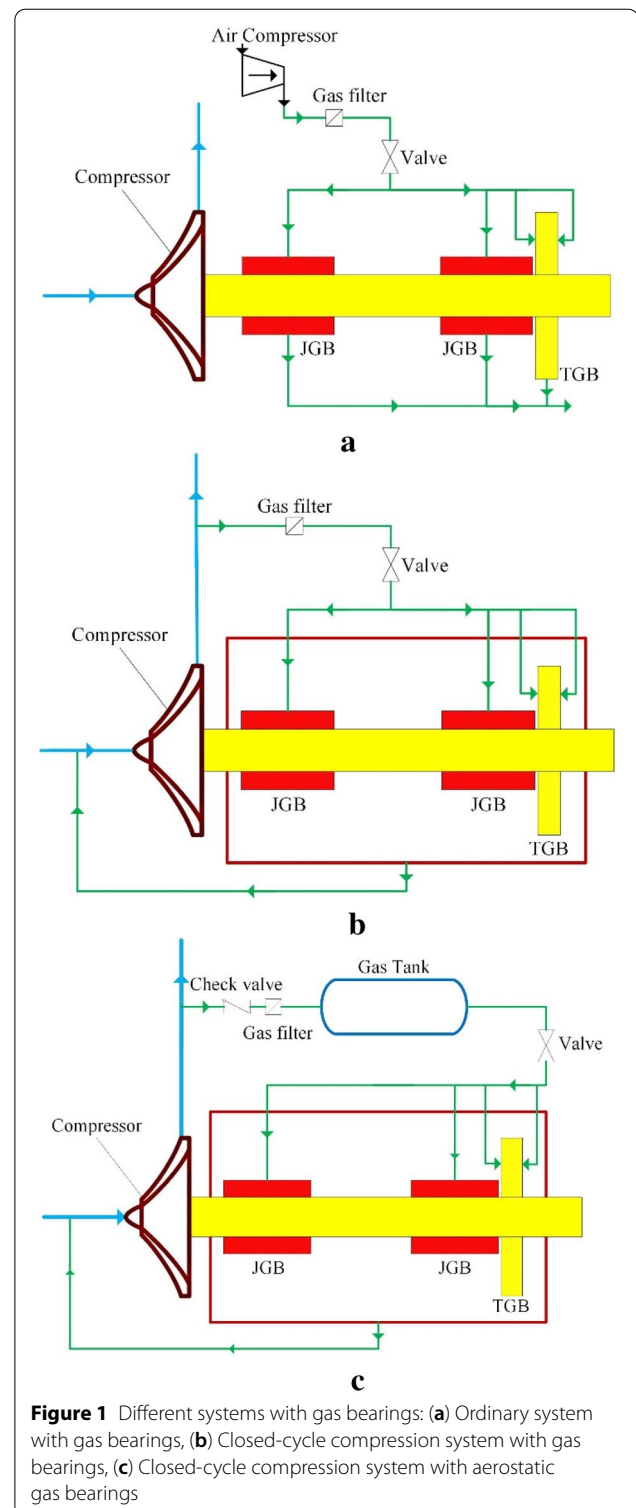
Figure 1 Different systems with gas bearings: (**a**) Ordinary system with gas bearings, (**b**) Closed-cycle compression system with gas bearings, (**c**) Closed-cycle compression system with aerostatic gas bearings

streams constitute an open-cycle that is independent of the main gas stream. The external air compressor provides the high-pressure gas that is supplied to the gas bearings. Therefore, the gas bearings can withstand the

Lian *et al. Chin. J. Mech. Eng.* (2020) 33:98

Page 3 of 16

rotor's loads in the system during the start-up process. However, the external air compressor increases the system's quality, but its complexity as well.

Figure 1(b) shows a closed-cycle compression system with gas bearings. Compared to the ordinary system with gas bearings, it decreases the external air compressor. After flowing through the compressor, the working medium becomes a high-pressure gas that can supply pressure for the gas bearings. Thus, a part of the pressurized gas is separated to supply the gas bearings so they can withstand the loads of the rotors in the system after flowing through the gas filter and valve. This portion of gas becomes a low-pressure gas after it flows through the gas bearings, and then it is collected and flows into the main stream for the next cycle.

This structure simplifies the system's composition. However, because of the rotor's low rotational speed and the compressor's low pressure ratio, the gas bearings that the gas supplies through the compressor are insufficient to withstand the rotor's loads. This causes dry friction between the rotor and gas bearings that affects the gas bearing's life.

The new start-up method of a closed-cycle compression system with aerostatic gas bearings is shown in Figure 1(c). An aerostatic gas bearing is chosen to support the rotor in this system. Moreover, a gas tank and a check valve are added compared to the previous system. The check valve is placed in front of the gas filter to prevent the high-pressure gas in the gas tank from flowing back during the start-up and stopping process. The gas tank is placed between the gas filter and the valve, which stores the pressurized gas to supply the rotor during the start-up process until the system is operating normally.

The system's specific start-up process is as follows.

Open the valve in the system after the gas tank and start the rotor until the gas bearings operate. The pressure of the gas in the gas tank decreases, while the rotor's rotational speed increases. Because of that phenomenon, the compressor's pressure ratio increases as the rotor's rotational speed increases; the pressurized gas flowing through the compressor will have higher pressure than the gas in the gas tank after the rotational speed exceeds a certain speed. After flowing through the check valve and the gas filter, a part of the pressurized gas is separated to supplement the gas in the gas tank. Once the rotational speed reaches the rated speed, the compressor's pressure ratio becomes stable, and the start-up process ends until the pressure of the gas in the gas tank is stable.

When the system works normally, the gas supplied to the gas bearings is still separated from the pressurized gas through the compressor, and flows through the gas tank first, compared to the previous system. At this time, the gas tank also serves as a pressure regulator, which enhances the pressurized gas's pressure stability and increases the gas bearings' life.

3 Mathematical Model and Test Bench
3.1 Modeling Assumptions
Although this start-up system is simpler, it still is too complex to model. Simplifications and assumptions related to the model are applied as follows:
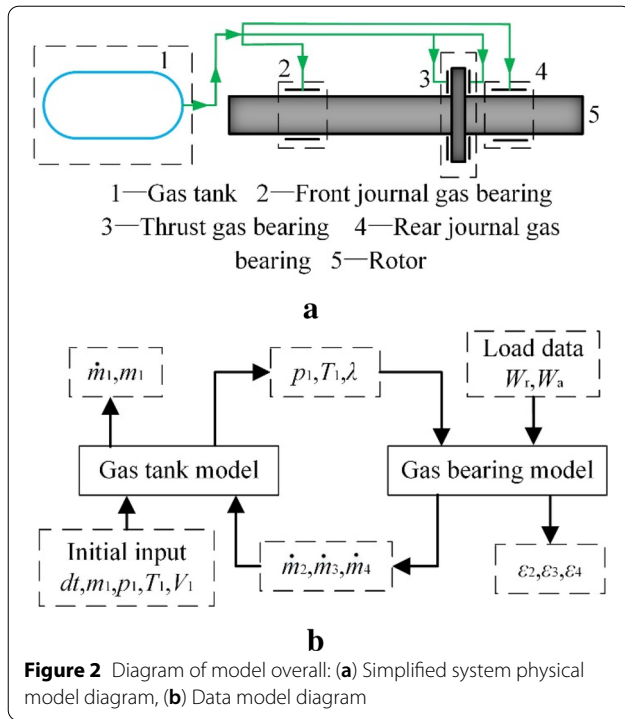
(1) Ignore the pressure loss attributable to the gas tank's shape.
(2) Fix the radial and axial loads, while ignoring the change of loads as the rotational speed changes.
(3) Assume that the rotor is a rigid body.
(4) Ignore the rotational speed's influence on the gas bearings' characteristics.
(5) Assume the pressure loss between the gas tank and air bearing is a fixed loss coefficient, λ.
(6) Assume that the gas bearings' supply pressure is equal.
(7) No supplement from the compressor to the gas tank, and compare only the start time and the bearing's working duration.

3.2 Model Overall
Based on the simplifications and assumptions above, the excess parts can be removed, and the remainder of the system can be separated into five parts: the rotor, gas tank, front journal gas bearing, rear journal gas bearing, and a pair of thrust gas bearings, which constitute the mathematical model. The simplified system is shown in Figure 2(a).

Because of the similarity of the method used to model the journal and thrust gas bearing, they are combined in the analysis. Under the assumptions in Section 3.1, only the rotor's gravity is considered in the model. As shown in Figure 2(b), the mathematical model overall can be divided into the following two main subcomponents: the gas tank model and the gas bearing model. The two subcomponents interact with each other by core parameters: the gas tank model outputs the gas pressure and temperature, and the pipeline's pressure loss coefficient as the inputs of the gas bearing model; the gas bearing model outputs each gas bearing's mass flow rate as the input of the gas tank model. The initial inputs of the model overall are the gas tank volume, the gas pressure and temperature, and the mass in the gas tank.

The specific relation between the gas tank model outputs and the gas bearings model's corresponding parameters is as follows:

Lian *et al. Chin. J. Mech. Eng.* (2020) 33:98

Page 4 of 16

Figure 2 Diagram of model overall: (**a**) Simplified system physical model diagram, (**b**) Data model diagram

Table 1 Initial inputs of the start-up model

Parameter	Value
Time step dt (s)	0.1
Initial gas pressure p_1^0 (MPa)	0.6
Initial gas temperature T_1^0 (K)	300

$$p_2 = p_3 = p_4 = p_1 \cdot \lambda, \tag{1}$$

$$T_2 = T_3 = T_4 = T_1. \tag{2}$$

Similarly, the equation for the gas bearing model's outputs and the corresponding parameters is as follows:

$$\dot{m}_1 = \dot{m}_2 + \dot{m}_3 + \dot{m}_4. \tag{3}$$

The initial inputs of the start-up model include time step, gas tank volume, radial and axial loads, initial gas pressure and temperature, and initial mass in the gas tank. Among these parameters, gas tank volume, and radial and axial loads are set as the arguments; initial mass in the gas tank can be calculated by the gas tank volume and the initial gas pressure and temperature; others are set as shown as Table 1.

The start-up time allowable is defined to measure the bearing working duration. Further, the allowable start-up time's definition is the time from which

the simulation of the start-up process begins until the point when the eccentricity of any gas bearing reaches 0.9, with the assumption that the compressor does not supplement the start-up process. Then, the rotor's start time and the start-up time allowable are compared to evaluate the start-up method' feasibility.

3.3 Gas Tank
Under the assumption in Section 3.1, a zero-dimensional model can be established to simulate the gas tank. The core parameters of the gas tank include its volume, gas pressure and temperature, and the mass in the gas tank, as well as the gas tank's mass flow rate. The governing equation can be written as follows:

$$\Delta m_1 = m_1 \cdot dt, \tag{4}$$

$$q \cdot dt = \Delta(m_1 \cdot u_1) - \Delta m_1 \cdot h_1, \tag{5}$$

$$p_1 V_1 = m_1 R_g T_1, \tag{6}$$

where Δm_1 represents the mass change in the gas tank in one time step, q represents the heating power to the gas tank, u_1 represents the internal energy of gas in the gas tank, h_1 represents the gas enthalpy, and the working medium is assumed to be the ideal gas.

The iterative equations used to solve the gas pressure and temperature and the mass can be obtained with Eqs. (4)–(6), as follows:

$$p_1^{n+1} = \frac{m_1^{n+1} \cdot R_g \cdot T_1^{n+1}}{V_1}, \tag{7}$$

$$T_1^{n+1} = T_1^n + \frac{q \cdot dt}{m_1^{n+1} \cdot c_v} - \frac{\dot{m}_1^n \cdot dt \cdot R_g \cdot T_1^n}{m_1^{n+1} \cdot c_v}, \tag{8}$$

$$m_1^{n+1} = m_1^n + \dot{m}_1^n \cdot dt, \tag{9}$$

where ϕ^n represents the parameter in the nth time step, and q is assumed as the constant.

However, if $q = 0$(the gas tank is non-heating), Eq. (8) can be simplified as follows:

$$T_1^{n+1} = T_1^n - \frac{\dot{m}_1^n \cdot dt \cdot R_g \cdot T_1^n}{m_1^{n+1} \cdot c_v}. \tag{10}$$

3.4 Gas Bearings
The gas bearing model is based largely on the mapping between the working condition and the bearing capacity, where the working condition includes supply pressure and eccentricity, and the bearing capacity includes load

Lian *et al. Chin. J. Mech. Eng.* (2020) 33:98

Page 5 of 16

capacity and mass flow rate. Therefore, the gas bearing model can be established as an empirical model.

Using the journal bearing as an example, the mapping between the working condition and the bearing capacity can be expressed as follows:

$$W = f(p, \varepsilon), \tag{11}$$

$$\dot{m} = f(p, \varepsilon). \tag{12}$$

However, the gas bearing model's inputs are the supply pressure in the nth time step, which is written as p^n, and the radial load. With known p^n, Eq. (11) can be written as follows:

$$\varepsilon^n = g^n(W_r^n), \tag{13}$$

where $g^n(x)$ represents the mapping between the known radial load and the unknown eccentricity in the nth time step when the supply pressure is p^n, and the W_r^n is known.

The eccentricity, ε^n, and mass flow rate, $\dot{m}^n$, are obtained by combining Eqs. (12) and (13).

The thrust bearing's modeling method is similar to that of the journal bearing. However, the thrust bearing always is designed in pairs in the system, such that the total bearing capacity is the sum of each single-sided thrust bearing's capacity. The relation of the clearance between each single-sided thrust bearing's bearing surfaces can be expressed as follows:

$$h_{31} + h_{32} = 50 \; \mu\text{m}, \tag{14}$$

where h_{31} and h_{32}, respectively, represent the clearance between each single-sided thrust bearing's bearing surfaces.

Nowadays, the CFD has become a popular tool to investigate the static [29, 30] and dynamic [31] performance, and to optimize the structure [32, 33]. Thus, to obtain the gas bearing empirical model, Fluent is employed to simulate the gas bearings, and the three-dimensional models of the flow filed are developed. In the simulations, the gas is considered compressible. The air is assumed to obey ideal gas law, but R134a is assumed to obey real gas law. The gas flow is assumed to be laminar and in the isothermal flow condition. The supply temperature is set as 300 K.

The schematic diagram of the journal gas bearing is shown in Figure 3(a); journal gas bearings' core geometry parameters include bearing diameter and length, feed orifice diameter and length, the orifices' distance from the end of bearings, their number per row, and mean radial clearance. The accurate values of these parameters are shown in Table 2, which are set equal to those recorded during experimental tests. A refined structured
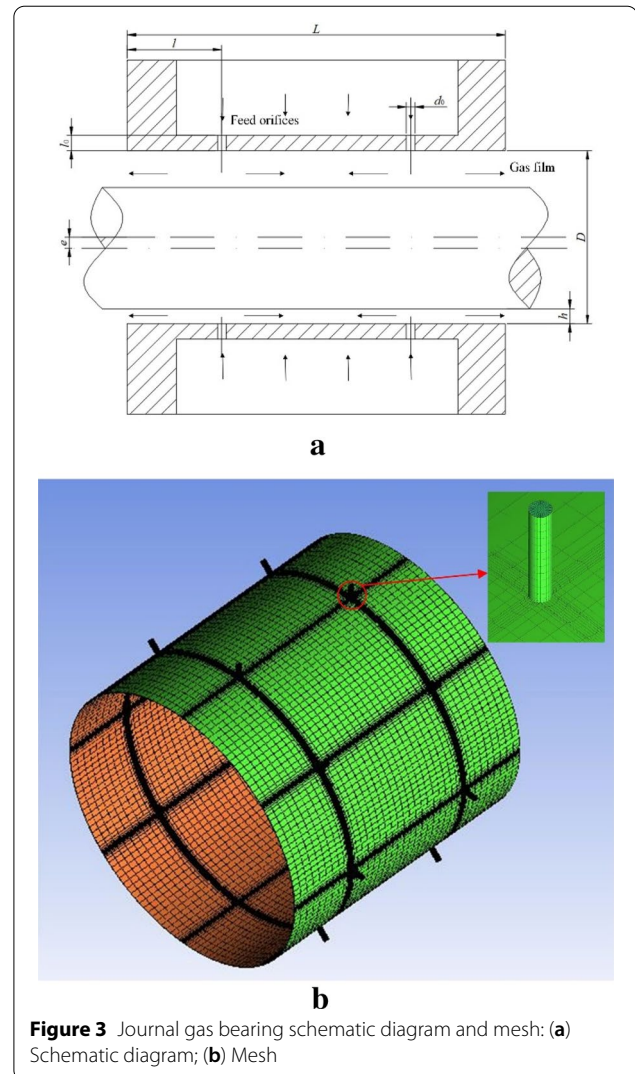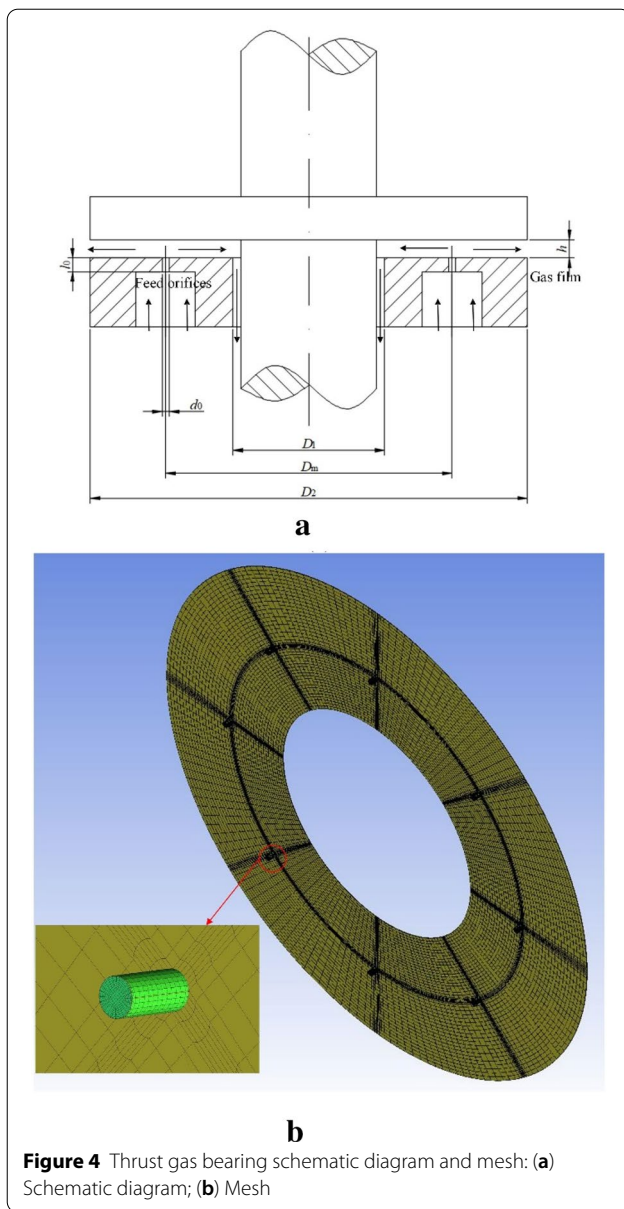

Figure 3 Journal gas bearing schematic diagram and mesh: (**a**) Schematic diagram; (**b**) Mesh

Table 2 Journal gas bearing parameters

Parameter	Value
Bearing diameter D (mm)	28
Bearing length L (mm)	28
Feed orifice length l_0 (mm)	1.5
Feed orifice diameter d_0 (mm)	0.6
Feed orifices' distance from end of bearings l (mm)	7
Feed orifice number per row N	8
Mean radial clearance h_0 (μm)	25

mesh is applied close to the feed orifices and gas film, as shown in Figure 4(b). Considering the precision and computing time, there are 280,000 hexahedral cells in the mesh. Upstream of the flow is assumed to have constant gauge pressure equal to the feed orifices inlets' supply

Lian *et al. Chin. J. Mech. Eng.*   (2020) 33:98

Page 6 of 16

Figure 4 Thrust gas bearing schematic diagram and mesh: (**a**) Schematic diagram; (**b**) Mesh

Table 3 Thrust gas bearing parameters
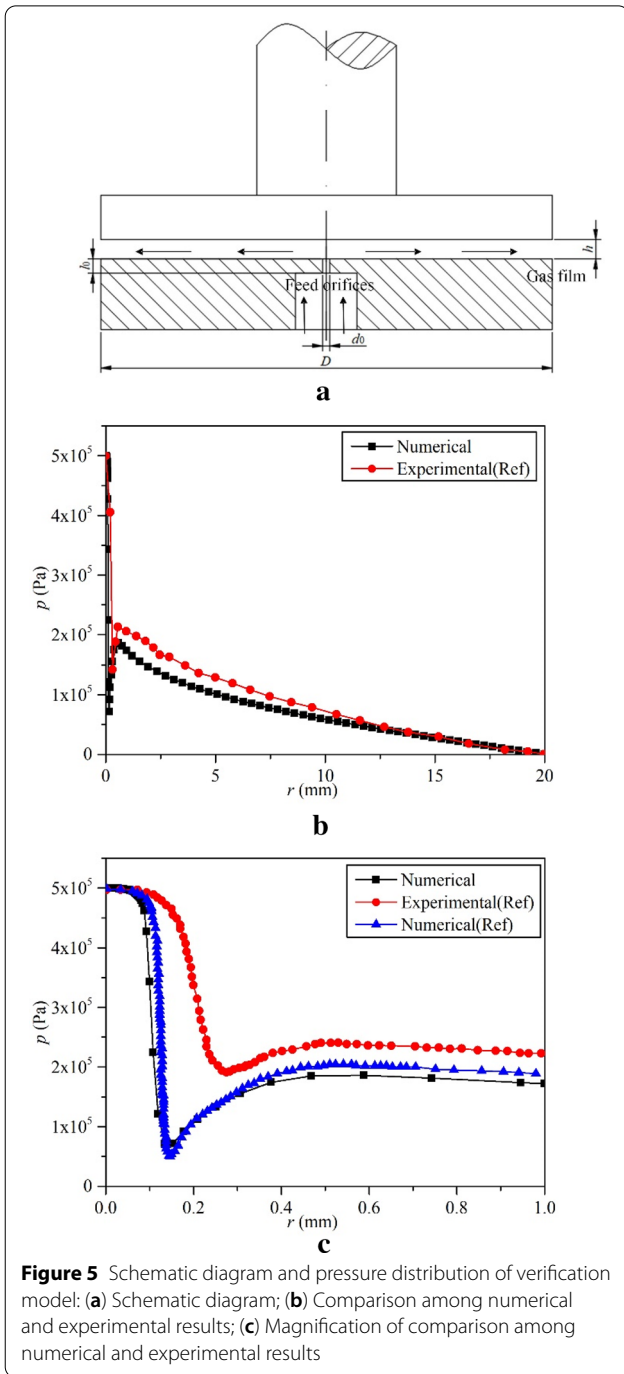
Parameter	Value
Bearing interior diameter D_1 (mm)	29
Bearing exterior diameter D_2 (mm)	65
Feed orifice length l_0 (mm)	1.5
Feed orifice diameter d_0 (mm)	0.6
Diameter of ring of feed orifices D_m (mm)	45
Feed orifice number N	8

to those recorded during experimental tests. A refined structured mesh is applied close to feed orifices and gas film, as shown in Figure 5(b). Considering the precision and computing time, there are 330000 hexahedral cells in the mesh. Upstream of the flow is assumed to have constant gauge pressure equal to the feed orifices inlets' supply pressure; downstream of the flow is set at atmospheric pressure. Moreover, the clearance between bearing surfaces, whose symbol is *h*, is the argument of the simulation model of the thrust gas bearings, and its range is 2.5 μm to 47.5 μm. Another argument is the supply pressure, which ranges from 0.2 MPa to 0.7 MPa.

To verify the correctness of gas bearings' simulation, a single-orifice thrust gas bearing, with the same geometry as that investigated in Ref. [5], is also evaluated using the Fluent. As shown in Figure 5(a), the core parameters includes bearing diameter *D* equal to 40 mm, feed orifice length l_0 equal to 0.3 mm, feed orifice diameter d_0 equal to 0.2 mm, the clearance between bearing surfaces *h* equal to 14 μm. Figure 5(b) shows the comparison of the pressure distribution along the gas film between the numerical and experimental results with a gauge supply pressure equal to 0.5 MPa and Figure 5(c) shows the comparison of the pressure distribution close to feed orifice with same boundary. Numerical results show a good agreement with the experimental ones, and the error is mainly caused by the sharp edge between the wall of the feed orifice and the bearing surface in numerical model, while experimental thrust bearings have a fillet or a chamfer between the wall of the feed orifice and the bearing surface, which was investigated by Belforte in Ref. [34].
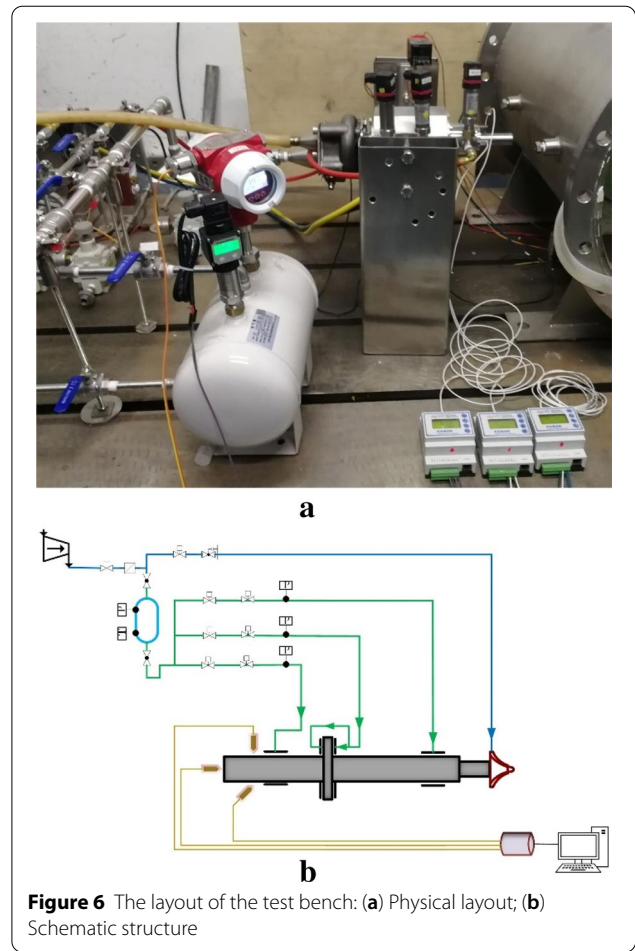
3.5 Test Bench

As shown in Figure 6, the working medium is air, and the air compressor supplies the pressurized air. The pressurized air is divided into two parts, one of which is connected to the gas tank to supply the pressurized air, while the other is connected to the turbine, which drives the rotor. Before the experiment, the air compressor supplements the air to the gas tank until the gas pressure reaches the initial pressure. At the beginning of the

pressure; downstream of the flow is set at atmospheric pressure. The supply pressure and the eccentricity are the arguments of the simulation model of journal gas bearing, and their ranges are 0.2 MPa to 0.7 MPa and 0.1 to 0.9, respectively.

The schematic diagram of the thrust gas bearing is shown in Figure 4(a). The bearing shown in the figure is annular and single-sided, so the thrust gas bearings' core geometry parameters include its interior and exterior diameter, feed orifice length and diameter, clearance between bearing surfaces, diameter of the feed orifices' ring, and feed orifice number. The accurate value of these parameters is shown in Table 3, which also are set equal

Lian *et al. Chin. J. Mech. Eng.* (2020) 33:98

Page 7 of 16

Figure 5 Schematic diagram and pressure distribution of verification model: (**a**) Schematic diagram; (**b**) Comparison among numerical and experimental results; (**c**) Magnification of comparison among numerical and experimental results

Figure 6 The layout of the test bench: (**a**) Physical layout; (**b**) Schematic structure

sensors with ranges of 0–1 MPa. The gas temperature in the tank is measured by a temperature sensor with ranges of 0–100 °C. Three eddy current displacement sensors with a range of 500 μm are applied to measure the axial and radial displacement of the rotor.

The gas tank's mass flow rate and journal bearings' radial eccentricity are measured indirectly. The gas pressure and gas temperature in the gas tank are measured directly, then gas density in the gas tank can be obtained. And the mass in the gas tank can be obtain, cause the gas tank volume is constant. Finally, the gas tank's mass flow rate will be calculated by Eq. (15):

$$\dot{m}^n = \frac{m_1^{n+1} - m_1^n}{dt} = \frac{\frac{p_1^{n+1}}{RT_1^{n+1}}V_1^{n+1} - \frac{p_1^n}{RT_1^n}V_1^n}{dt}. \quad (15)$$

The journal bearings' radial displacement Δx is measured directly. Then, the journal bearings' radial eccentricity can be calculated by Eq. (16):

experiment, we open the valve connecting the gas tank and the gas bearings to allow the gas bearings to operate. After ensuring they are working, the valve connected to the turbine is opened to drive the rotor at a low speed to protect the gas bearing.

Figure 6(b) shows the structure scheme of the test bench. The gas pressure in the gas tank and the supply pressure of gas bearings are measured by four pressure

Lian *et al. Chin. J. Mech. Eng.*   (2020) 33:98

Page 8 of 16

$$\varepsilon = 1 - \frac{\Delta x}{h_0}. \tag{16}$$

4 Results and Analysis
4.1 Gas Bearing Simulation Results
4.1.1 Journal Gas Bearing
The journal bearing's bearing capacity can be obtained by fixing the geometric parameters and then changing the supply pressure and eccentricity.

Figure 7 shows the journal gas bearing's simulation results under different supply pressures and eccentricities when the working mediums are air and R134a, respectively.

Figure 7(a) and (b) show the load capacity under different operating conditions, which shows that the designed journal bearing's load capacity is similar under different working mediums. It can be determined

that the load capacity varies nonlinearly with the eccentricity when the supply pressure is constant. At a deep level, when $\varepsilon \geq 0.8$, the load capacity nearly always increases slightly.

Figure 7(c) and (d) show the mass flow rate under different working conditions. It can be seen that the eccentricity has little influence on the mass flow rate, while the supply pressure is the key factor that influences the rate. Moreover, the mass flow rate under R134a is twice as fast as under air.
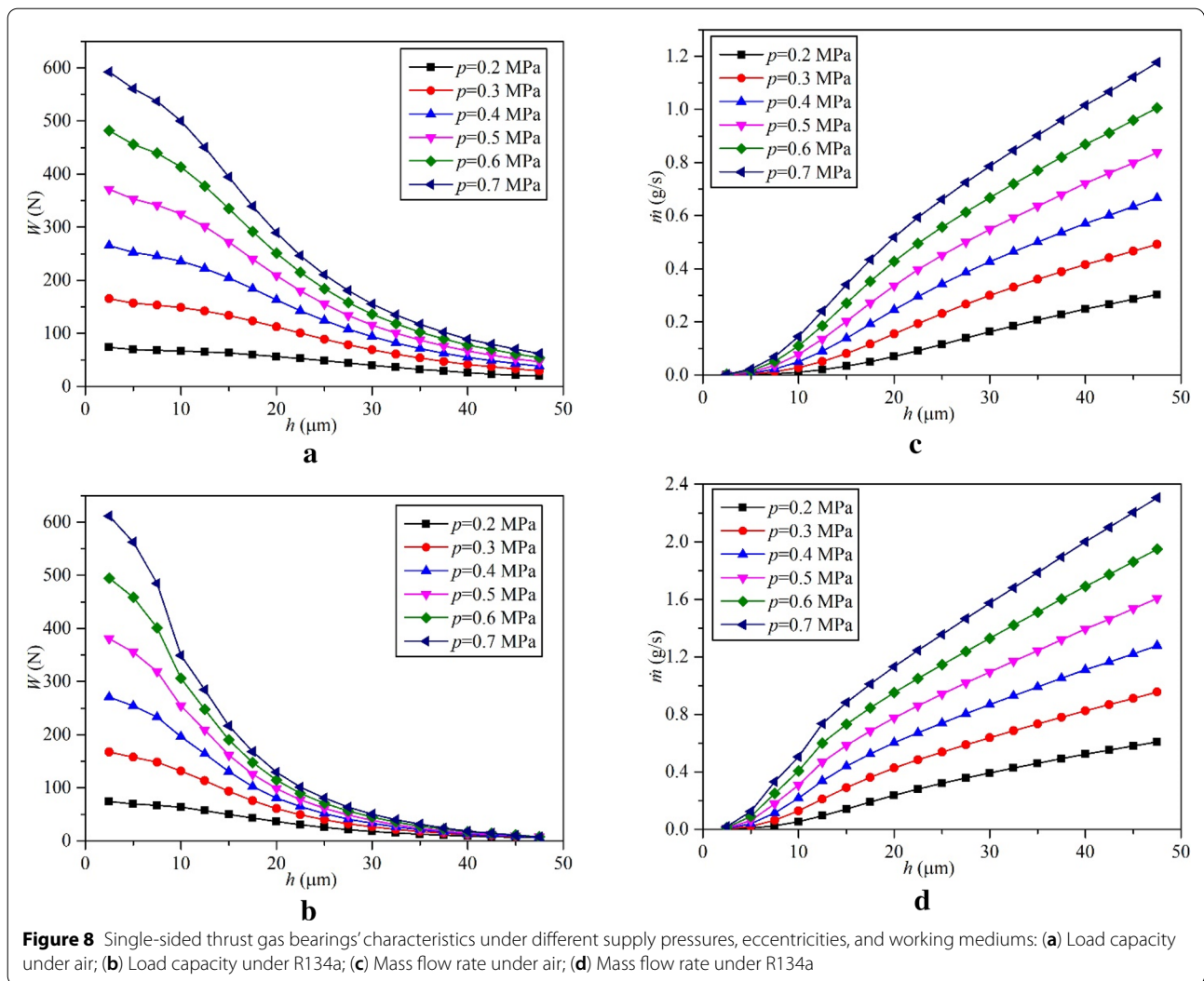
4.1.2 Thrust Gas Bearing
The single-sided thrust bearing's bearing capacity can be obtained by fixing the geometric parameters, except the clearance between the thrust bearing surfaces, and then changing the supply pressure and the clearance.

Figure 8 shows the single-sided thrust bearing's load capacity and mass flow rate, respectively, under different

Figure 7 Journal gas bearings' characteristics under different supply pressures, eccentricities, and working mediums: (**a**) Load capacity under air; (**b**) Load capacity under R134a; (**c**) Mass flow rate under air; (**d**) Mass flow rate under R134a

Figure 8 Single-sided thrust gas bearings' characteristics under different supply pressures, eccentricities, and working mediums: (**a**) Load capacity under air; (**b**) Load capacity under R134a; (**c**) Mass flow rate under air; (**d**) Mass flow rate under R134a

working conditions. However, the form expressed for the single-sided thrust bearing's capacity differs from that expressed for the journal bearing's capacity, which needs to be processed to obtain the unified form.

As Section 3.4 reports, single-sided thrust bearings always are designed in pairs, and the clearance between each bearing's bearing surfaces can be described as Eq. (14). Thus, we define the thrust bearing's eccentricity analogous to that of the journal bearing. The definition of the thrust bearing's eccentricity can be expressed as follows:

$$\varepsilon = \frac{\left| h_{31} - h_{32} \right|}{h_{31} + h_{32}}. \tag{17}$$

Figure 9 shows the thrust bearing's load capacity and mass flow rate, respectively, under different working conditions after processing, which have the unified form and similar performance as do the diagrams showing the journal bearings' capacity.

4.1.3 Influence of the Supply Temperature
Having defined the supply pressure at 0.3 MPa, the journal gas bearing's eccentricity at 0.5, and the clearance between the thrust gas bearing surfaces at 15 μm, further simulations are carried out with a series of varying supply temperature in a range from 280 K to 300 K to analyze the relation between the gas bearings' performance and supply temperature.

Figure 9 Thrust gas bearings' characteristics under different supply pressures, eccentricities, and working mediums: (**a**) Load capacity under air; (**b**) Load capacity under R134a; (**c**) Mass flow rate under air; (**d**) Mass flow rate under R134a
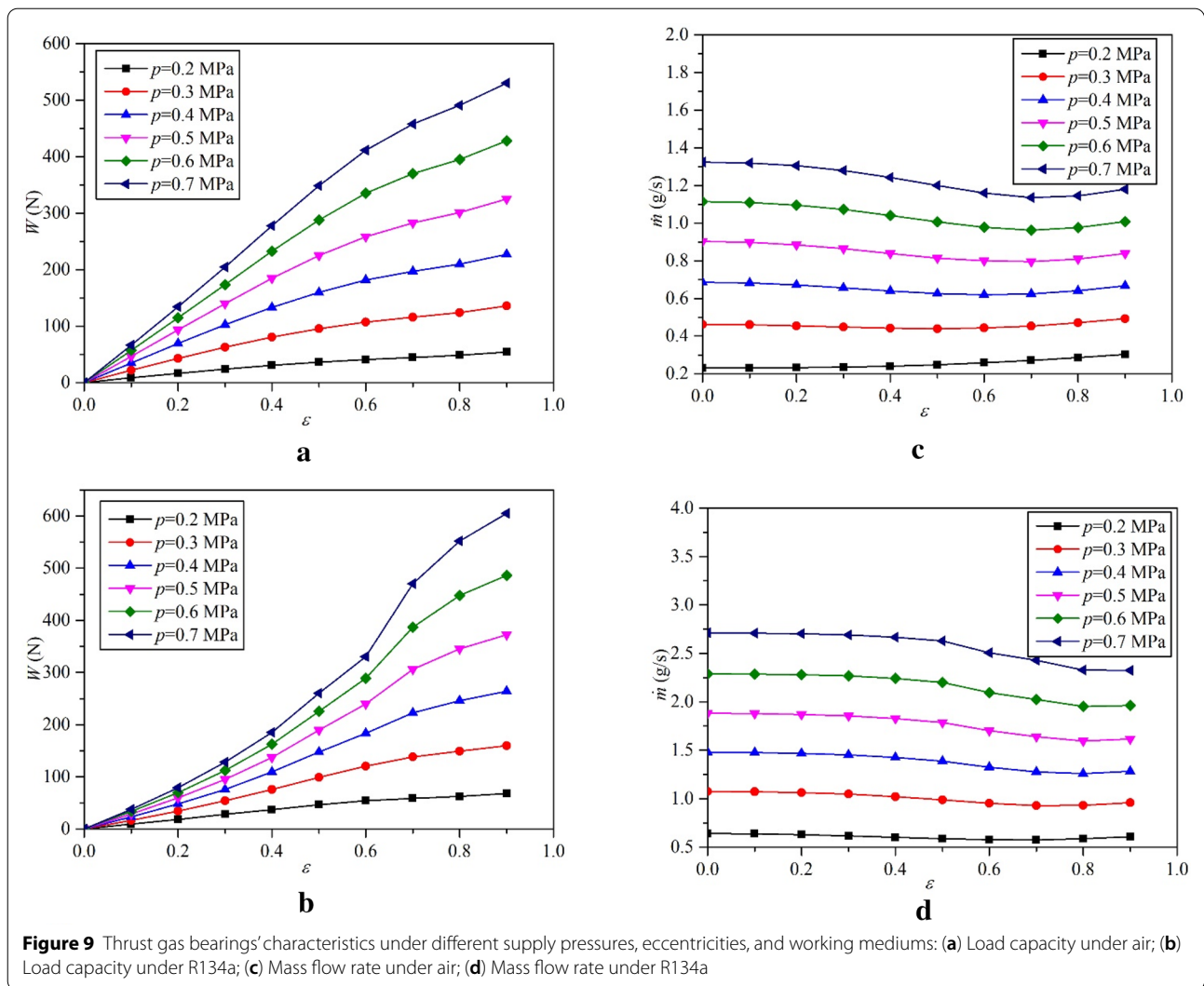
Figure 10 shows supply temperature's influences on the gas bearings' load capacity and mass flow rate. It can be seen that the two are nearly independent of the supply temperature, which indicates that it is unnecessary to set gas bearings' performances as a function of supply temperature. Thus, it is possible to use the gas bearings' performances shown in Sections 4.1.1 and 4.1.2 to predict the model's performance overall, and the error of mass flow rate will be less than 7.9%, while the error of load capacity will be less than 5.2%.

4.2 Results of Start-Up Model
4.2.1 Gas Tank Volume
The gas tank volume is the key factor that affects the start-up method's feasibility. A gas tank that is too small will cause a rapid reduction in the supply pressure, which results in insufficiency of the bearings' load capacity, abrasion between the rotor and bearings, failure of the

start-up process, and decreased bearing life. At the same time, while a gas tank that is too large can be used for the start-up process, it affects the working efficiency of other system components.

Fixing the radial load as $W_r = 50$ N, which indicates that the radial load on each journal gas bearing is 25 N, and the axial load as $W_a = 150$ N, the system's performance under different working mediums during the start-up process can be examined.

Figure 11 shows gas pressure changes in the gas tank during the start-up process. It can be seen that the gas tank volume is approximately directly proportional to the start-up time allowable, which proves that increasing the gas tank volume is an effective way to enhance the start-up method's feasibility.

Comparing Figure 11 (a) and (b), it can be seen that the start-up time allowable under R134a is longer than that under air. Under the same supply pressure level, the gas

Lian *et al. Chin. J. Mech. Eng.*   (2020) 33:98

Page 11 of 16

Figure 10 Gas bearings' characteristics under different supply temperature: (**a**) Load capacity; (**b**) Mass flow rate

Figure 11 Gas pressure in the gas tank during the start-up process under different gas tank volumes and working mediums: (**a**) Air, (**b**) R134a
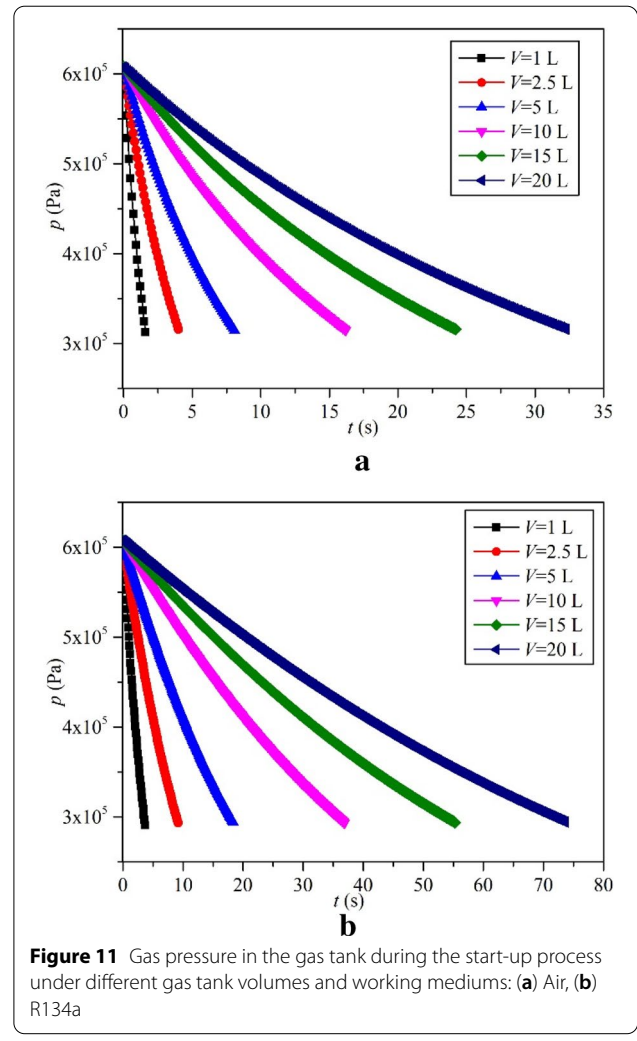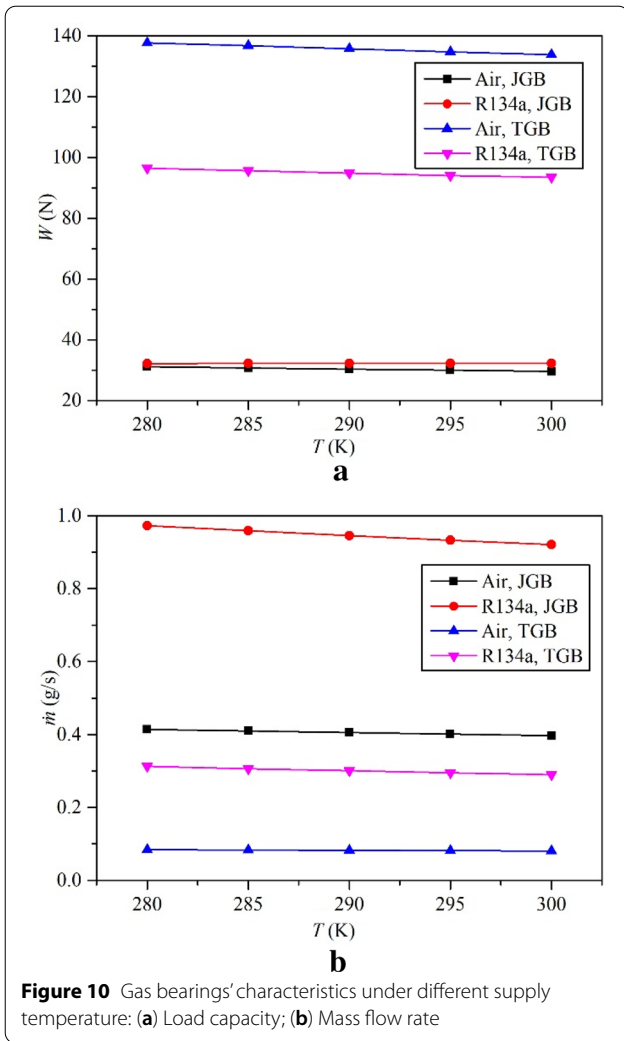
bearings' mass flow rate under R134a is greater than that under air, and their proportionality constant is approximately 2:1. However, R134a's density is three times that of air, so the gas tank can store more R134a than air. This indicates that the percentage of mass flow rate and mass in the gas tank are smaller under the same initial pressure when the working medium is R134a.

Figure 12 shows each gas bearing's eccentricity during the start-up process. The dotted lines in the figure represent thrust gas bearings' eccentricity, while the solid lines represent that of journal gas bearings. It can be seen that the journal gas bearing performs better than does the thrust gas bearing in two ways: the thrust gas bearing's eccentricity reaches 0.9 in every working condition, and its initial eccentricity is higher than that of the journal gas bearing.

The first explanation for the result is that the single-sided thrust bearings affect each other when they are designed in pairs, which leads to the load capacity loss

and bidirectional axial load capacity. However, the journal bearings share the radial load, which increases the load capacity. The second explanation for the result is that the axial load is greater than the radial load. Moreover, the axial load is selected as the compressor's axial force under the rated working condition, which is larger than the actual axial load.

Comparing Figure 12(a) and (b), it can be seen that each gas bearing's initial eccentricity is higher under R134a. This indicates that a gas bearing's load capacity under air is greater than under R134a at a low eccentricity, which is also shown in Figure 9. As the gas pressure in the gas tank decreases, the eccentricities become higher, and the gas bearings' load capacities under R134a gradually become greater than those under air, which increases the start-up time allowable.

Lian *et al. Chin. J. Mech. Eng.*   (2020) 33:98

Page 12 of 16
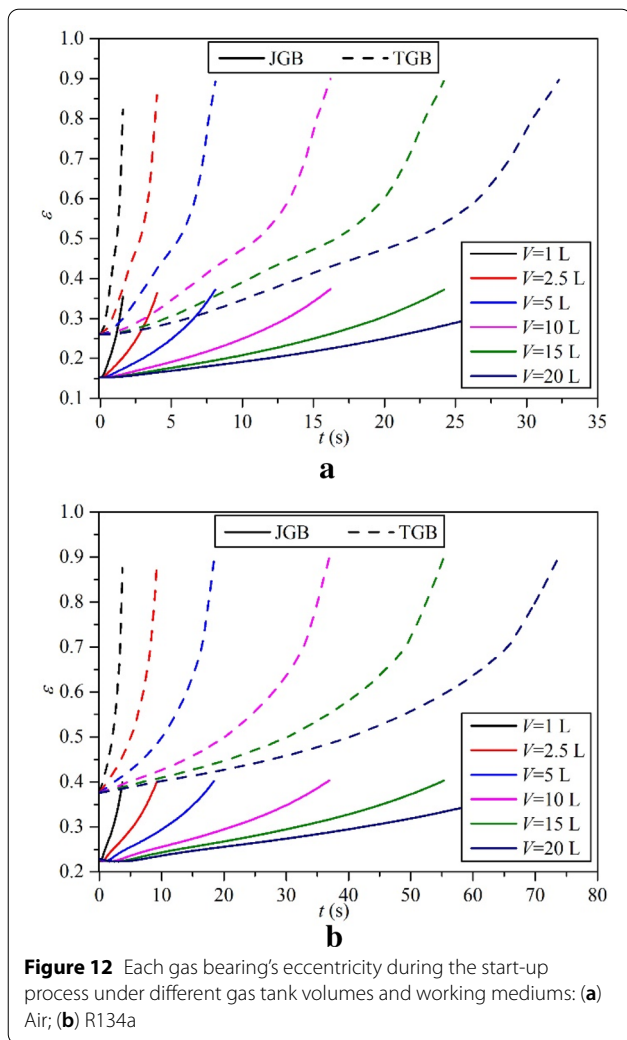
Figure 12 Each gas bearing's eccentricity during the start-up process under different gas tank volumes and working mediums: (**a**) Air; (**b**) R134a
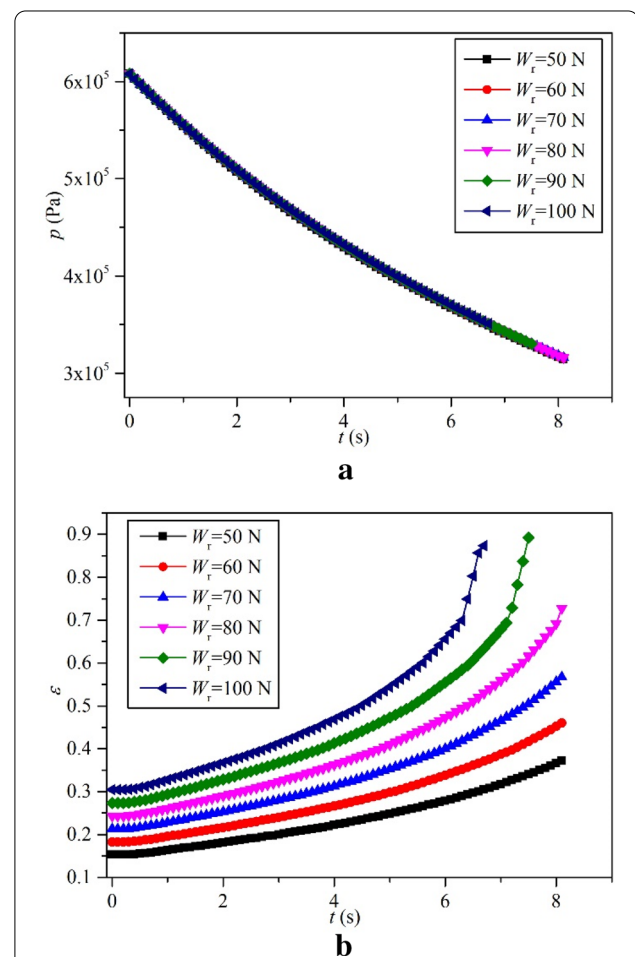
$$t = \frac{n\pi J}{30 Tar}, \tag{18}$$

where n represents the motor's rated speed, the unit of which is r/min, J represents the rotor's moment of inertia, the unit of which is $kg \cdot m^2$, and Tar represents the motor's average starting torque, the unit of which is $N \cdot m$.

The accurate values of these parameters are determined as the motor itself is designed, and are shown as Table 4.

Combine Table 4 and Eq. (18), we obtain: $3.34 \leq t \leq 7.34$. Thus, the start-up time allowable must be greater than this value to guarantee the start-up method's feasibility. After comparison, it can be shown that the gas tank volume must be greater than 5 L under air, which affects other components little, while its volume must be greater than 2.5 L under R134a.

Figure 13 Characteristics during the start-up process under different radial loads: (**a**) Gas pressure in gas tank; (**b**) Journal gas bearings' eccentricity

To evaluate the start-up method's feasibility, the rotors' start time should be compared with the start-up time allowable.

Assume that the motor drives the system. Then, the rotors' start time is the same as that of the motor. The motor's start time can be calculated with the following equation:

Table 4 Motor parameters

Parameter	Value
Motor's rated speed n (r/min)	80000
Rotor's moment of inertia J (kg·m²)	3.6787×10^{-4}
Motor's rated torque T (N·m)	0.42
Motor's average starting torque Tar (N·m)	$k \cdot 0.42$, $k \leq 2.2$

Lian *et al. Chin. J. Mech. Eng.*   (2020) 33:98

Page 13 of 16

4.2.2 Radial and Axial Load

Section 4.2.1 indicates that the axial load causes the thrust gas bearing's eccentricity to reach 0.9 first, when $W_r = 50$ N, and $W_a = 150$ N. This indicates that the appropriate increase of radial load may not influence the start-up method's feasibility. Therefore, we should fix the gas tank volume as $V = 5$ L and axial load as $W_a = 150$ N to set the radial load as an argument to study the radial load's influence.

Figure 13(a) shows the gas pressure in the gas tank under different radial loads. The change in radial loads affects the change in gas pressure only slightly. However, when the radial load exceeds a critical value, the increased radial load causes the allowable start-up time to decrease. The explanation of this phenomenon is shown in Figure 13(b).

Figure 13(b) shows the journal gas bearing's eccentricity under different radial loads. The thrust gas bearing's eccentricities are not shown, because they are the same as those shown in Figure 12(b). As the radial load increases, the journal gas bearing's eccentricity increases in every time step, and the thrust gas bearing's eccentricity reach 0.9 first when $W_r \leq 80$ N. However, when $W_r > 80$ N, the journal gas bearing's eccentricity will reach 0.9 first; therefore, the journal gas bearing becomes the key component of the start-up method. In addition, it can be seen that the journal gas bearing's eccentricity increases rapidly when it is above 0.7, which is caused by a small increase in the load capacity. Accordingly, the journal gas bearing's eccentricity should be set below 0.7 by adjusting other components in the gas bearing system design.

Analogously, we fix the gas tank volume as $V = 5$ L and radial load as $W_r = 50$ N to set the axial load as an argument to determine the axial load's influence.
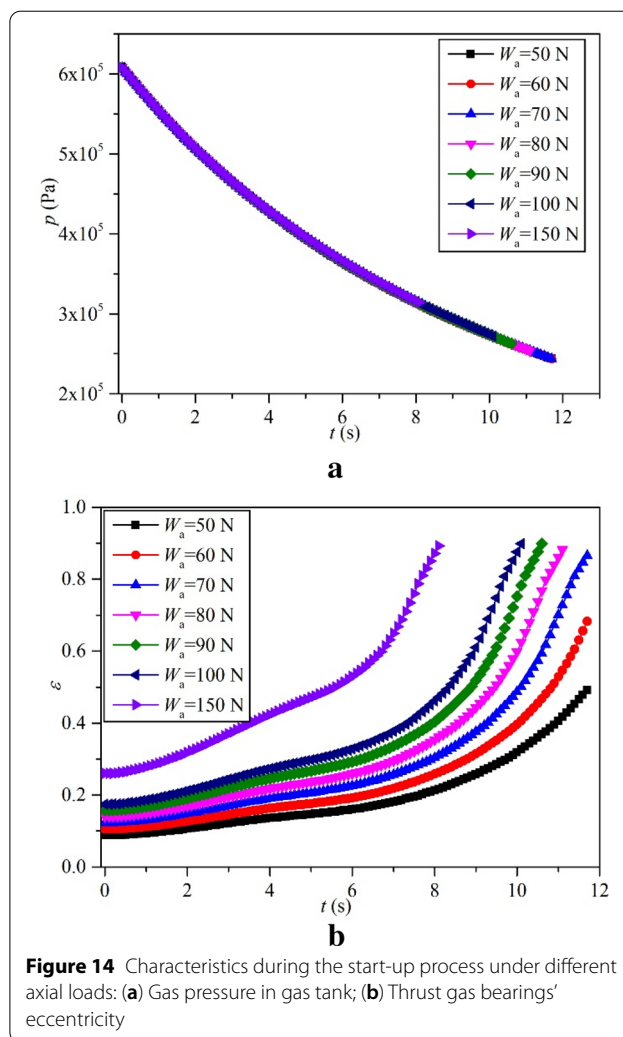
Figure 14(a) shows the gas pressure in the gas tank under different axial loads. It also can be seen that a small axial load affects the start-up process little, while a large axial load decreases the start-up time allowable.

Figure 14(b) shows the thrust gas bearing's eccentricity under different axial loads. The journal gas bearing's eccentricities reach 0.9 first when $W_a \leq 70$ N, while the thrust gas bearing's eccentricities will reach 0.9 first when $W_a > 70$ N.

The analysis of the radial and axial loads' influence will become one of the guidelines in designing the gas bearings and radial and axial loads.

4.3 Experimental Results

The gas tank volume is 5 L, and the rotor's quality is approximately 5 kg, which is identical to the simulation conditions.
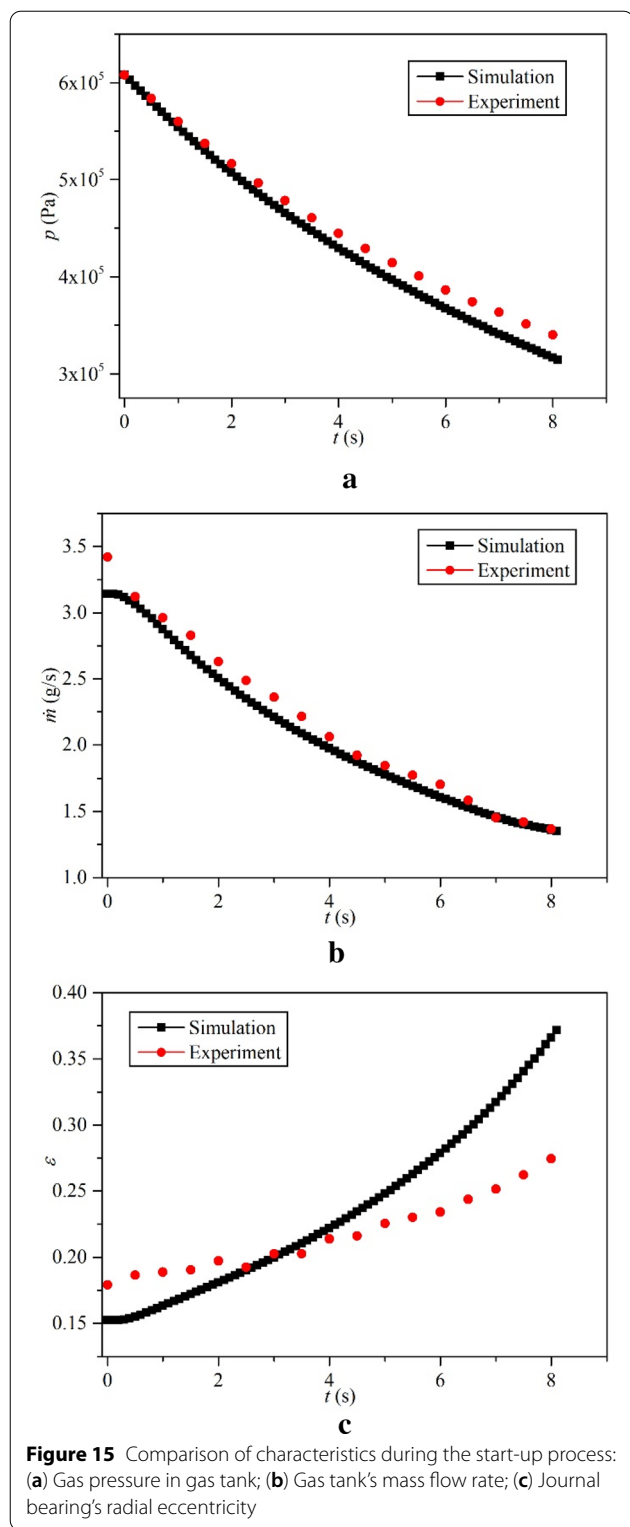

Figure 14 Characteristics during the start-up process under different axial loads: (**a**) Gas pressure in gas tank; (**b**) Thrust gas bearings' eccentricity

Figure 15(a) shows a comparison of the gas pressure in the gas tank between the experiment and simulation. It can be seen that the experimental gas pressure is higher than that in the simulation. That indicates that the experimental start-up time allowable is longer than that of the simulation. However, the largest error between the experimental and numerical gas pressure is 6.1%, which is small enough to prove that the simulation of the start-up method can match the true situation.

Figure 15(b) shows the comparison of the gas tank's mass flow rate between the experiment and the simulation. The experimental mass flow rate matches the numerical rate well, with the exception of the initial flow rate, the error of which is 8.9%.

Figure 15(c) shows the comparison of journal bearings' radial eccentricity between the experiment and the simulation. It can be seen that the change of experimental radial eccentricity is similar with the numerical. The error mainly comes from three factors: numerical error of

Figure 15 Comparison of characteristics during the start-up process: (**a**) Gas pressure in gas tank; (**b**) Gas tank's mass flow rate; (**c**) Journal bearing's radial eccentricity

gas bearing discussed in Section 3.4, pipeline's pressure loss and the error of gas pressure in the gas tank. All gas bearing in the test bench have a fillet or chamfer between their feed orifice's wall and bearing surface, instead of

an ideal sharp edge, which causes the numerical error. At the beginning of the experiment, the gas tank's mass flow rate is large, and the pipeline's pressure loss is larger than the calculated, which results that the experimental journal bearings' radial eccentricity larger than the calculated. After the 5th second, the experimental gas pressure in the gas tank is higher than the calculated, as shown in Figure 15(a), which results that the experimental journal bearings' radial eccentricity smaller than the calculated. Nevertheless, the experimental radial eccentricity over time agrees well with the numerical result.

5 Conclusions

In this paper, we address the previous start-up methods and existing problems of closed-cycle compression systems with gas bearings. To solve those problems, we propose a new start-up method that involves the same system, but with aerostatic gas bearings, which reduces the system's complexity and increases the bearings' life.

Then, we model the new start-up method and simulate a specific example with accurate values to analyze the start-up method's feasibility and the characteristics during the start-up process. The gas tank volume is approximately directly proportional to the start-up time allowable. When the other parameter is determined, the model can predict a sufficiently small gas tank, which not only ensures the feasibility of start-up, but also affects other components only minutely.

The radial and axial loads also influence the characteristics during the start-up process. When one of them is fixed, the model can predict the largest possible size of the other, which makes the start-up time allowable as long as possible, such that the model can predict a perfect combination of radial and axial loads.

The working medium is another factor that influences characteristics during the start-up process. R134a is more suitable as the working medium of the system analyzed, because the start-up time allowable under R134a is longer than that under air. The model also can distinguish the best working medium from among the alternatives.

Further, the test bench is built to verify the simulation. The experimental results agree strongly with numerical results, and the experimental start-up time allowable is slightly longer than the numerical one, which indicates that the numerical predictions may not need to be amended as a safety factor.

However, the model requires predicting the stability and unbalanced response of gas bearings during the start-up process, on which our future research will focus.

Abbreviations

Acknowledgements

Authors' Contributions

Authors' Information
Huaqi Lian, born in 1994, is currently a PhD candidate at *National Key Laboratory of Science and Technology on Aero Engines Aero-thermodynamics & Collaborative Innovation Center for Advanced Aero-Engine, School of Energy and Power Engineering, Beihang University, China*. He received his bachelor degree from *Beihang University, China*, in 2016. His research interest includes spacecraft thermal control.

Hong Wu, born in 1971, is currently a professor and a PhD candidate supervisor at *National Key Laboratory of Science and Technology on Aero Engines Aero-thermodynamics & Collaborative Innovation Center for Advanced Aero-Engine, School of Energy and Power Engineering, Beihang University, China*.

Yulong Li, born in 1987, is currently an associate professor and a PhD candidate supervisor at *National Key Laboratory of Science and Technology on Aero Engines Aero-thermodynamics & Collaborative Innovation Center for Advanced Aero-Engine, School of Energy and Power Engineering, Beihang University, China*. His research interests include spacecraft thermal control and distributed electric propulsion. Tel: +86-10-82317694.

Chengjun Rong, born in 1989, is currently a PhD candidate at *National Key Laboratory of Science and Technology on Aero Engines Aero-thermodynamics & Collaborative Innovation Center for Advanced Aero-Engine, School of Energy and Power Engineering, Beihang University, China*.

Funding

Competing Interests

References

[1] Q Gao, W Q Chen, L H Lu, et al. Aerostatic bearings design and analysis with the application to precision engineering: State-of-the-art and future perspectives. *Tribology International*, 2019, 135: 1-17.

[2] T Raparelli, V Viktorov, F Colombo, et al. Aerostatic thrust bearings active compensation: Critical review. *Precision Engineering*, 2016, 44: 1-12.

[3] T Wu, X R Meng, X L Wei, et al. Design and performance analysis of a radial inflow turbogenerator with the aerostatic bearings for organic Rankine cycle system. *Energy Conversion and Management*, 2020, 214: 1-18.

[4] L Lentini, M Moradi, F Colombo. A historical review of gas lubrication: From Reynolds to active compensations. *Tribology in Industry*, 2018, 40(2): 165-182.

[5] G Belforte, T Raparelli, V Viktorov, et al. Discharge coefficients of orifice-type restrictor for aerostatic bearings. *Tribology International*, 2007, 40: 512-521.

[6] L Y Song, K Cheng, H Ding, et al. Analysis on discharge coefficients in FEM modeling of hybrid air journal bearings and experimental validation. *Tribology International*, 2018, 119: 549-558.

[7] J B Zhang, D L Zou, N Ta, et al. A numerical method for solution of the discharge coefficients in externally pressurized gas bearings with inherent orifice restrictors. *Tribology International*, 2018, 125: 156-168.

[8] X Q Zhang, X L Wang, R Liu, et al. Influence of temperature on non-linear dynamic characteristic of spiral-grooved gas-lubricated thrust bearing-rotor systems for microengine. *Tribology International*, 2013, 61: 138-143.

[9] J B Zhang, D L Zou, N Ta, et al. Numerical research of pressure depression in aerostatic thrust bearing with inherent orifice. *Tribology International*, 2018, 123: 385-396.

[10] J L Schwartz, M A Peck, C D Hall. Historical review of air-bearing spacecraft simulators. *Journal of Guidance Control and Dynamics*, 2003, 26(4): 513-522.

[11] M Ciarcia, R Cristi, M M Romano. Emulating scaled Clohessy-Wiltshire dynamics on an air-bearing spacecraft simulation tested. *Journal of Guidance Control and Dynamics*, 2017, 40(10): 2496-2510.

[12] Y Y Li, G Lei, Y Sun, et al. Effect of environmental pressure enhanced by a booster on the load capacity of the aerodynamic gas bearing of a turbo expander. *Tribology International*, 2017, 105: 77-84.

[13] T Ise, M Nakatsuka, K Nagao, et al. Externally pressurized gas journal bearing with slot restrictors arranged in the axial direction. *Precision Engineering*, 2017, 50: 286-292.

[14] C W Zhang, D Z Zheng, Y W Seo, et al. The effect of a thermal contact sensor on the temperature distribution and heat flux at the disk surface. *Tribology International*, 2019, 131: 678-685.

[15] L L Gao, C Wu, D J Zhang, et al. Research on a high-accuracy and high-pressure pneumatic servo valve with aerostatic bearing for precision control systems. *Precision Engineering*, 2019, 60: 355-367.

[16] C Dellacorte, M J Valco. Load capacity estimation of foil air journal bearings for oil-free turbomachinery applications. *Tribology Transactions*, 2000, 43(4): 795-801.

[17] C Dellacorte, K C Radil, R J Bruckner, et al. Design, fabrication and performance of open source Generation I and II compliant hydrodynamic gas foil bearings. *Tribology Transactions*, 2008, 51(3): 254-264.

[18] K C Radil, C Dellacorte. A three-dimensional foil bearing performance map applied to oil-free turbomachinery. *Tribology Transactions*, 2010, 53(5): 771-778.

[19] E Guenat, J Schiffmann. Real-gas effects on aerodynamic bearings. *Tribology International*, 2018, 120: 358-368.

[20] A Patel, A K Balasubramanian, V Biradar, et al. Analysis of aerostatic thrust bearing for S-CO2 turbomachinery. *6th ASME Gas Turbine India Conference*, Chennai, India, December 5-6, 2019: 1-6.

[21] E R Marsh, D A Arneson, M J Liebers, et al. Effects of gas composition on asynchronous error motion in externally pressurized spindles. *Precision Engineering*, 2008, 32(2): 143-147.

[22] M H Briggs, J M Prahl, R Bruckner, et al. High pressure performance of foil journal bearings in various gases. *STLE/ASME 2008 International Joint Tribology Conference*, Miami, Florida, October 20-22, 2009: 403-405.

[23] T M Conboy. Real-gas effects in foil thrust bearings operating in the turbulent regime. *Journal of Tribology*, 2013, 135(3): 1-6.

[24] J Demierre, A Rubino, J Schiffmann. Modeling and experimental investigation of an oil-free microcompressor-turbine unit for an organic rankine cycle driven heat pump. *Journal of Engineering for Gas Turbines and Power*, 2015, 137(3): 1-10.

[25] E Guenat, J Schiffmann. Thin gas film isothermal condensation in aerodynamic bearings. *Journal of Tribology*, 2019, 141(11): 1-8.

[26] C W Zhang, X Q Jiang, L Q Wang, et al. Effect of surface roughness on the start-stop behavior of air lubricated thrust micro-bearing. *Tribology International*, 2018, 119: 436-442.

[27] K Feng, W H Liu, R Yu, et al. Analysis and experimental study on a novel gas foil bearing with nested compression springs. *Tribology International*, 2017, 107: 65-76.

Lian *et al. Chin. J. Mech. Eng.*   (2020) 33:98

Page 16 of 16

[28] B Ruan. Numerical modeling of dynamic sealing behaviors of spiral groove gas face seals. *Journal of Tribology*, 2002, 124(1): 186-195.

[29] R Z Yan, L Y Wang, S Z Wang. Investigating the influences of pressure-equalizing grooves on characteristics of aerostatic bearings based on CFD. *Industrial Lubrication and Tribology*, 2019, 71(7): 853-860.

[30] K Ishibashi, A Kondo, S Kawada, et al. Static and dynamic characteristics of a downsized aerostatic circular thrust bearing with a single feed hole. *Precision Engineering*, 2019, 60: 448-457.

[31] H Zhuang, J G Ding, P Chen, et al. Numerical study on static and dynamic performances of a double-pad annular inherently compensated aerostatic thrust bearing. *Journal of Tribology*, 2019, 141(5): 1-14.

[32] Y F Li, Y H Yin, H Yang, et al. Micro-vibration analysis and optimization of aerostatic bearing with pocketed orifice-type restrictor. *Journal of Applied Fluid Mechanics*, 2018, 11(4): 1115-1124.

[33] Y F Li, Y H Yin, H Yang, et al. Modeling for optimization of circular flat pad aerostatic bearing with a single central orifice-type restrictor based on CFD simulation. *Tribology International*, 2017, 109: 206-216.

[34] G Belforte, T Raparelli, A Trivella, et al. CFD analysis of a simple orifice-type feeding system for aerostatic bearings. *Tribology Letters*, 2015, 58(2): 1-8.